Detection of channel-hillslope coupling along a tectonic gradient

Martin D. Hurst[a,*], Stuart W. D. Grieve[b], Fiona J. Clubb[c], Simon M. Mudd[d]

[a]*School of Geographical and Earth Sciences, University of Glasgow, Glasgow, UK, G12 8QQ*
[b]*School of Geography, Queen Mary University of London, London, UK, E1 4NS*
[c]*Department of Geography, Durham University, Durham, UK, DH1 3LE*
[d]*School of GeoSciences, University of Edinburgh, Edinburgh, UK, EH8 9XP*

Abstract

Landscape morphology reflects the spatial and temporal history of erosion. Erosion in turn embodies the competition between tectonic and climatic processes. Quantitative analysis of topography can therefore reveal the driving tectonic conditions that have influenced landscape development, when combined with theoretical understanding of erosion processes. Recent developments in the automated analysis of high-resolution ($<$ 10 m) topographic data mean that integrated analysis of hillslope and channel topographic metrics can provide understanding of the transient response of landscapes to changing boundary conditions. We perform high-resolution topographic analysis of hillslopes and channels in small ($<$ 3 km^2) catchments spanning an inferred uplift gradient along the Bolinas Ridge, California, USA, revealing tight coupling between channel steepness and hillslope metrics thought to be proxies for erosion rates. We find that the concavity of channel longitudinal profiles varies inversely with uplift rates, although drainage density increases with uplift rates. Both of these

[*]Corresponding author
Email address: `martin.hurst@glasgow.ac.uk` (Martin D. Hurst)

results can be explained by the contribution of mass wasting processes to valley formation in steeper (high uplift rate) landscapes. At the catchment scale, hillslope and channel metrics for erosion are correlated, hillslopes and channels steepen in concert, and hilltops (ridges) get sharper with increased uplift rate. This broad agreement suggests that hillslopes are responding to erosion rates in the channel network, which implies that landscape uplift is relatively stable and prolonged. Hillslope morphology deviates systematically from the steady-state predictions of established geomorphic transport laws, suggesting that hillslope adjustment is ongoing and that relief is growing.

1. Introduction

Understanding the dynamic interactions between mountain building and erosion has been a key goal of geomorphological research [e.g. 1]. The topographic form of hillslopes and rivers has been suggested to reflect competing influences:

5 tectonic processes generally tend to increase relief due to differential uplift [e.g. 2], whereas erosion and weathering processes generally act to subdue relief. Advances in the collection of topographic data now allow us to quantify and delineate Earth surface processes at both greater spatial scales and higher resolutions than previously possible. Quantifying relationships between erosion and

10 topography using these data therefore provides the potential to understand the tectonic conditions that have influenced landscape development [3].

Previous research has focused independently on how channel morphology [e.g. 4, 5, 6, 7, 8] or hillslope morphology [e.g. 9, 10, 11, 12] reflect rates of erosion,

2

and by inference, tectonics. Transient signals, resulting from changing boundary

conditions such as the rate of tectonic uplift, are conveyed through the landscape

along rivers by the upstream migration of steepened reaches called knickzones

or knickpoints [2]. Fluvial channels set the base-level conditions for hillslopes

[13, 10, 9], and therefore hillslope response to erosion rate variations should

lag behind that of channels [14, 9]. Hillslope response to faster erosion rates

results in increased hillslope sediment flux or more frequent mass movements

[15], and hillslope materials in turn may aid or inhibit river incision [e.g. 16].

The hilltop (or ridge) should be the last part of the landscape to respond,

as the transient adjustment migrates upslope from the base of the hillslope

to the divide [17]. Therefore, channels, hillslopes, and hilltops all have the

potential to archive information about the nature of landscape development

[17, 18]. The response timescales of these components of the landscape, however,

are inherently different. Coupling analysis of these process domains should allow

us to investigate the timescale of landscape response to transient signals from

topographic data alone.

Despite channel incision serving as the driver in hillslope evolution models

[e.g. 14], no study, to our knowledge, has explicitly linked key proxies of hillslope

erosion such as hilltop curvature [19, 9], hillslope length [11], or divergence from

steady-state predictions [19, 17] to the steepness of individual channels in order

to identify transience in landscape evolution and explore evidence for changes in

uplift rates in space and time. In this study we used techniques for extracting

channel and hillslope properties from high resolution topography [9, 20, 21]

3

to probe the coupling of hillslopes and channels along the Bolinas Ridge in California, where previously both spatial and temporal variations in rock uplift have been inferred [6].

2. Topographic indicators of landscape evolution

2.1. Channel steepness

Early work suggested that channel steepness may reflect erosion rates. However, as stated by G.K. Gilbert in his *Report on the Geology of the Henry Mountains* [22]: "In general we may say that, *ceteris paribus*, declivity bears an inverse relation to quantity of water" (p. 114). In other words, we must normalize for the size of the stream to compare channel steepness between different drainage basins, as headwaters will tend to be steeper than downstream reaches even if they are eroding at the same rate. There exists, generally, co–variation between channel slope and drainage area that can be broadly described by a power law relationship [23]:

$$S = k_s A^{-\theta} \tag{1}$$

In Equation (1), S is the local channel slope, k_s is called the steepness index, as it sets the overall gradient of the channel, A is the drainage area (often used as a proxy for discharge) in $[\mathrm{L}^2]$ (dimensions expressed in terms of [L]ength, [M]ass and [T]ime), and θ [dimensionless] is referred to as the concavity index since it describes how concave a profile is: the higher the value, the more rapidly channel gradient decreases downstream. The dimensions of k_s depend on the value of θ

4

$[\mathrm{L}^{-2\theta}]$, but both can be estimated by regressing S against A, since Equation (1) predicts a linear relationship between S and A in logarithmic space. Many studies have found that erosion rates are positively correlated with k_s values [e.g. 7, 24, 25].

Extracting k_s and θ directly from topographic data is challenging because slope data can be noisy, which prompted Royden and colleagues [26] to develop a method that compares the elevations of channel profiles, rather than slope. We can modify this approach to integrate Equation (1), since $S = dz/dx$ where z [L] is elevation and x [L] is distance along the channel [e.g., 27], resulting in

$$z(x) = z(x_b) + \left(\frac{k_s}{A_0{}^{\theta}}\right) \int_{x_b}^{x} \left(\frac{A_0}{A(x)}\right)^{\theta} dx, \qquad (2)$$

where A_0 is a reference drainage area that ensures the term within the integral in Equation (2) is dimensionless. We can then define a longitudinal coordinate, χ [L]:

$$\chi = \int_{x_b}^{x} \left(\frac{A_0}{A(x)}\right)^{\theta} dx. \qquad (3)$$

where x_b [L] is the flow distance at some arbitrary base-level. χ is defined such that at any point in the channel

$$z(x) = z(x_b) + \left(\frac{k_s}{A_0{}^{\theta}}\right)\chi. \qquad (4)$$

Equation (4) shows that k_s is the slope of the channel in χ–elevation space if A_0 is set to unity. In both Equation (1) and Equation (4), the numerical value of k_s depends on the value chosen for the concavity, θ. In order to compare

5

the steepness of channels in basins of different sizes, a reference concavity value
is typically chosen (θ_{ref}), which is then used to extract a normalized channel
steepness from the data [5]. We calculate θ values that minimize the variation
in χ–elevation profiles between tributaries and the trunk channel [26] using
a method that minimizes a disorder statistic [18, 28] and mismatches between
tributaries and trunk channels [29], which have previously been demonstrated to
best reproduce θ values in numerical landscapes [29]. Channel steepness is then
quantified for segments of the channel network, extracted using a statistical
method that calculates the most likely combination of channel segments by
rewarding goodness of fit but penalizing over parametrization of the segment
fitting [20].

2.2. Hillslope metrics

Hillslopes tend to be steeper in rapidly eroding landscapes. However, a
process transition has been demonstrated to occur in rapidly eroding terrain
that limits hillslope gradient [e.g. 30], resulting in hillslope gradients that are
decoupled from erosion rates [e.g. 24, 7]. Volumetric hillslope sediment transport
(per unit contour width) Q_s [L^2 T^{-1}] has been suggested to vary non-linearly
with hillslope gradient S [L L^{-1}] [30], such that sediment flux increases rapidly
approaching a limiting gradient S_C [L L^{-1}]:

$$Q_S = \frac{-D\,S}{\left(1 - \left(\frac{S}{S_C}\right)^2\right)}.\tag{5}$$

In Equation (5), D [L^2 T^{-1}] is a transport coefficient related to the efficacy

6

of sediment disturbing agents (such as burrowing organisms, tree throw, freeze-thaw cycling). Values of D vary with both substrate and climate [31].

Assuming that the hillslope has adjusted so that it is lowering at a constant rate along its length, in concert with erosion rate in the adjacent channel E [L T^{-1}] (in which case we say the hillslope is at steady-state), Equation (5) predicts that the Laplacian curvature at hilltops (i.e. topographic divides) C_{HT} [L^{-1}] is proportional to E:

$$E = -\frac{\rho_s}{\rho_r} D C_{HT}. \tag{6}$$

In Equation (6), ρ_s and ρ_r [M L^{-3}] are the bulk densities of dry soil and bedrock respectively. So, where the hillslope has had time to adjust to erosion rates in the adjacent channel, there should be correspondence between hillslope and channel metrics for erosion [9]. Conversely, where erosion rates in the channel have changed recently, the hillslope may be decoupled as it undergoes transient adjustment [17]. The response time of hillslopes to changes in boundary conditions is influenced predominantly by hillslope length L_H [L], the diffusivity coefficient D, and erosion rate E itself; hillslopes that are already eroding rapidly can respond quickly to a change in boundary conditions [14].

To allow comparison between hillslopes of different lengths and in landscapes with varying processes and climate regimes, we can normalize this relationship [19] to a reference erosion rate E_R [L T^{-1}]:

$$E_R = \frac{D S_C}{2 L_H (\rho_r/\rho_s)}, \tag{7}$$

7

in order to define a dimensionless erosion rate E^*:

$$E^* = \frac{E}{E_R} = \frac{-2\,C_{HT}\,L_H}{S_C}. \tag{8}$$

Hillslope relief R [L] (the elevation difference between the top and toe of a hillslope) can also be normalized with respect to the maximum theoretical relief on a hillslope as dictated by $S_C \times L_H$:

$$R^* = \frac{R}{S_C\,L_H}. \tag{9}$$

These normalizations allow hillslope morphology to be characterized in terms of a dimensionless erosion rate and dimensionless relief that are functions of measurable topographic parameters C_{HT}, L_H and S [9, 11]. This allows the derivation of the theoretical steady-state relationship between E^* and R^* [19]:

$$R^* = \frac{1}{E^*}\left(\sqrt{1 + [E^*]^2} - \ln\left(\frac{1}{2}\left[1 + \sqrt{[E^*]^2}\right]\right) - 1\right). \tag{10}$$

Where hillslopes are at steady-state, their morphology should be well described by Equation (10). However, if the channel incision rate changes, it will take some some for the entire hillslope to adjust. Relief will begin to respond immediately to changing incision rates at the hillslope base, but this signal takes some time to propagate to the hilltop, meaning that deviations from the steady-state curve will occur [17]. Positive departures in R^* (or negative deviations in E^*) from the steady-state curve indicate that the landscape is being rejuvenated, whereas negative offset in R^* (or positive E^*) from the steady-state curve suggests the hillslopes are decaying [17]. The time such perturbations

8

last depends on the change in incision rate but in most landscapes the peak divergence from the steady-state curve will last on the order of 10^3-10^4 years [32].

3. Setting

Section 2 shows that a range of channel, hillslope, and hilltop metrics have been developed that can link landscape morphology to erosion rates and therefore tectonics or climate. However, in order to couple these metrics to investigate the timescale of landscape response to perturbations, we need both high resolution topographic data and a landscape of sufficient scale that channel and hillslope metrics could vary both upstream as well as in adjacent basins. In addition, capturing the dynamic response of hillslopes as they lag behind channel adjustments requires a landscape with evidence for transient perturbation. We therefore chose to explore channel–hillslope coupling along the Bolinas Ridge in California, where an uplift gradient had previously been inferred based on channel steepness analysis [6].

The Bolinas Ridge, California, USA, is located adjacent to the San Andreas Fault (SAF) (Figure 1). The ridge is underlain predominantly by Cretaceous sandstones of the Franciscan Formation [33]. It is drained by a series of small catchments trending perpendicular to the SAF. Topographic relief increases along the length of the feature from north-west (NW) to south-east (SE). The steepness of the river channels generally increases from NW to SE and has been used to infer a gradient in uplift up to rates potentially exceeding 0.5 mm yr^{-1},
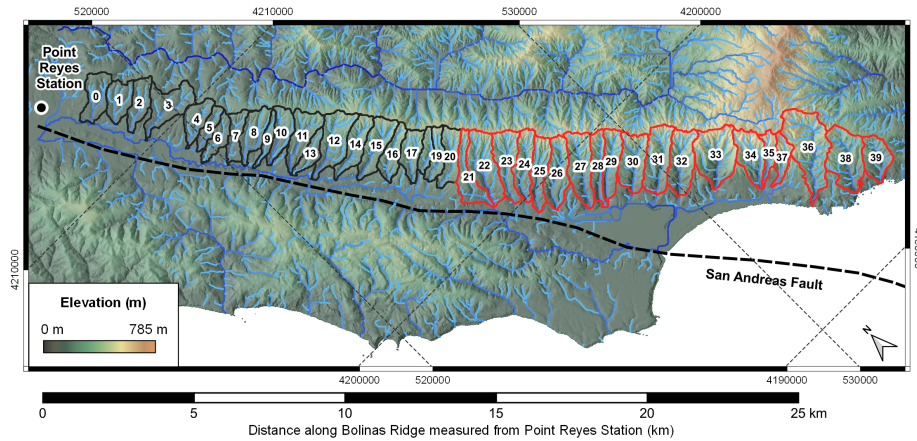
Figure 1: Study site along the Bolinas Ridge, Marin County, California, showing shaded relief and elevation. Outlined study catchments (numbered sequentially with distance along the Bolinas Ridge from Point Reyes Station) drain towards the San Andreas Fault, before draining along the fault either NW into Tomales Bay (black outlines) or SW into Bolinas Bay (red outlines). The stream network is shaded based on Strahler stream order with darker blue indicating higher order streams. Coordinate system is UTM Zone 10N.

with a 3–5× increase in rock uplift along the length of the ridge, with rates established within the last 1–3 Ma [6]. To the west of the SAF, OSL dating of marine terraces has also found higher uplift rates to the south near Bolinas Bay [34], although they caution that structures leading to differential uplift to the west of the fault are unlikely to propagate across the near–vertical SAF. Modern climate is maritime, warm summer Mediterranean with mean annual precipitation 1200 ± 400 mm yr^{-1} and mean annual temperature 14.2 ± 0.7 °C (PRISM Climate Group, Oregon State University, http://prism.oregonstate.edu [35]; averaged over 1895–2015; variability is 1σ). We focus our analysis on catchments of comparable size that drain towards the SAF (Figure 1).

10

4. Methods

We explore the spatial variability of topographic metrics along the length of
the Bolinas Ridge. The topographic data used was the USGS National Elevation

Dataset (NED) 1/9 arc second (`https://nationalmap.gov/elevation.html`),
projected to UTM Zone 10N to produce a 3 m resolution digital terrain model
(DTM).

4.1. Channel profile analysis

The location of the channel network was determined using a threshold in
contour curvature applied to a 3 m resolution digital terrain model (DTM) that
had been filtered using an optimal Wiener filter [36, 37, 21]. This method has
been found to successfully locate field-mapped channel heads to an accuracy of
~10-20 meters [37], and is relatively insensitive to grid resolution up to ~10
meters [38]. Steepest descent flow routing then defined the channel network
downstream of mapped channel heads (Figure 2). Drainage density was calcu-
lated for each catchment as the total length of channels divided by the catchment
area [12].

After extracting the channel network, we mapped the spatial distribution of
k_{sn} within each basin, which provides the opportunity to assess the distribution
of E. Royden and colleagues [26] suggested that changes in base-level can
be recorded in channel networks through the upstream migration of discrete
'patches' with distinct k_s values, reflecting local erosion rate if a value for θ
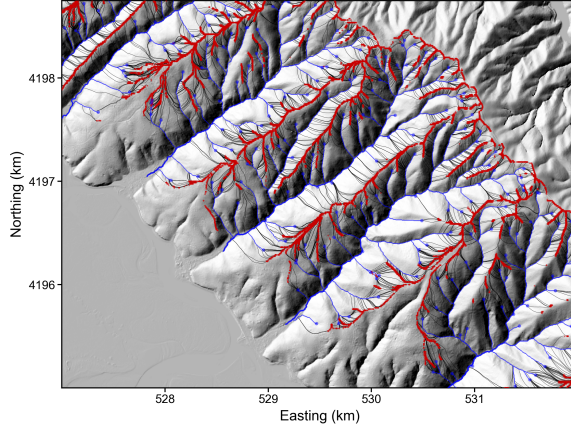can be estimated or assumed (with the potential to infer rates and processes of

11

Figure 2: Example section of the Bolinas Ridge showing the location of mapped channel heads (blue circles), the resulting channel network (blue lines), the hilltop network (red lines) and traces (black lines) along which hillslope morphology was extracted. Image is centered on catchments #31 and #32 (see Figure 1). Coordinate system is UTM Zone 10N.

surface uplift).

185   We estimated θ using routines developed by [29], which minimizes the difference between χ–elevation profiles of tributaries and the trunk channels within each catchment [see also 28]. This analysis was performed for every catchment along the Bolinas Ridge in order to derive a best fit θ value for the entire landscape, and also explore whether the most likely θ value varied with the inferred

190   uplift rate. We used a median θ value for the whole landscape as a reference concavity θ_{ref} in order to compute k_{sn} as a topographic proxy for erosion rates in the channel network.

12

We then computed the χ coordinate using a θ_{ref} value of 0.31 and used the statistical technique of [20] to extract the most likely segments of consistent k_{sn} values along the channel network. The segmented channel network was further divided to limit segments to 100 m in length in order to explore the spatial variation in topographic metrics throughout the landscape, but ensuring a meaningful sample size for each segment. Because channels set base-level conditions for hillslopes, we used recently developed methods (see below) to link ridge tops and hillslopes to their down-slope channel segments. This allows us to compare hillslope metrics with those associated with the local channel.

4.2. Extracting Hillslope Morphology

The locations of hilltops were determined using algorithms developed by Grieve et al. [21]. We extracted the channel network (Figure 2) and selected hilltops that are adjacent to two channels of the same Strahler stream order. Flow paths were traced down the steepest descent path from each individual hilltop pixel to the channel network [9, 21]. The channel segment at the toe of the hillslope trace was recorded allowing us to relate hillslope and channel morphology spatially.

For each trace C_{HT}, L_H and S were calculated in order to calculate E^* and R^* based on topography. The limiting slope gradient (S_C) was determined by iterating across a realistic range of values (0.5–1.2) and finding the value for which hillslope relief $R = L_H * S$ was less than the theoretical maximum hillslope relief $R_{max} = L_H * S_C$ for 99% of measured hillslope traces (Figure 3). According to Equation (5), hillslope sediment flux approaches infinity as
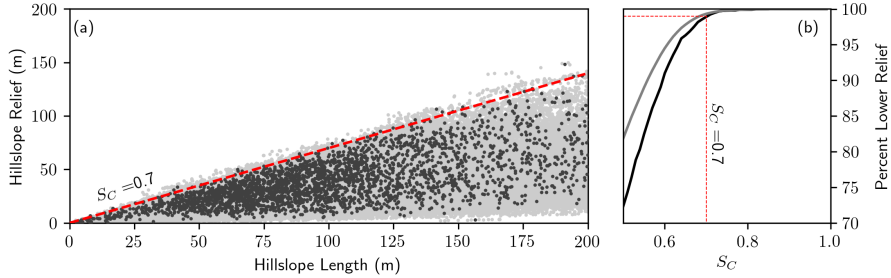
13

Figure 3: Determination of S_C based on hillslope morphology. (a) Plots of hillslope relief as a function of hillslope length for all individual hillslope traces (light gray) and median segmented hillslope data (dark gray). Dashed red line shows the maximum theoretical relief for $S_C = 0.7$. (b) This value was determined by iterating across possible S_C values to find a value for which 99% of all hillslopes had lower relief.

slope gradient S approaches the limiting slope gradient S_C, and thus hillslopes governed by Equation (5) should not be able to attain a gradient of S_C. We find a value of $S_C = 0.7$ is appropriate to the hillslopes along the Bolinas Ridge. This is at the lower end, but consistent with previous values recorded across a range of landscapes [11].

5. Results

5.1. Stream Network Topology and Topography

Drainage density initially increases linearly from NW to SE along the Bolinas Ridge as the channel network extends further upslope into the catchments (Figure 4a). However from roughly 15 km along the landform, drainage density no longer varies systematically with distance. The variation in drainage density corresponds to hillslope length, with shorter hillslopes in catchments with

14

higher drainage density (Figure 4b). Conversely, the two catchments with the steepest channels have relatively low drainage density.
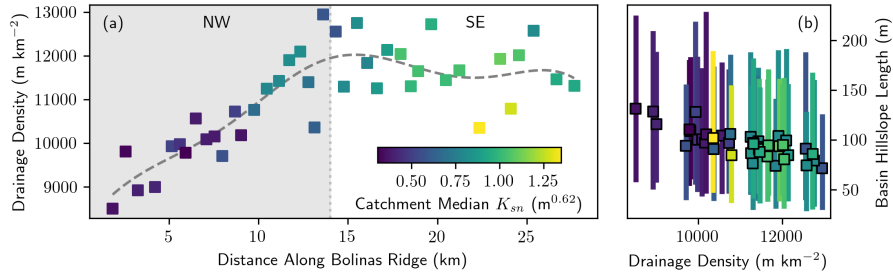

Figure 4: (a) Variation in catchment drainage density along the length of the Bolinas Ridge from NW to SE (distance from Point Reyes Station), color-coded by catchment-median channel steepness index (θ_{ref}=0.31). D_D increases with distance until ~15 km along the landform. (b) Variation in hillslope length (median and 16th–84th percentile range L_H) with D_D showing an inverse relationship.

²³⁰ Estimates of channel steepness in Figure 4 depend on the use of a reference concavity, but concavity may vary systematically in transient landscapes [29]. We found that channel concavity generally declines along the length of the Bolinas Ridge from NW to SE (Figure 5a), with lowest concavities coinciding with the zone with the highest k_{sn}, where maximum uplift has been inferred [6], ²³⁵ though there is considerable scatter (Figure 5b). This declining trend is statistically significant as demonstrated by a Mann-Kendall test (p values of 2×10^{-5} and 0.015 for the disorder and bootstrap concavity methods respectively). The bootstrap method [29] resulted in lower estimates of θ than the disorder method [28], but the spatial pattern is similar for both.

²⁴⁰ Taking a reference concavity of $\theta_{ref} = 0.31$ (the median of all values from
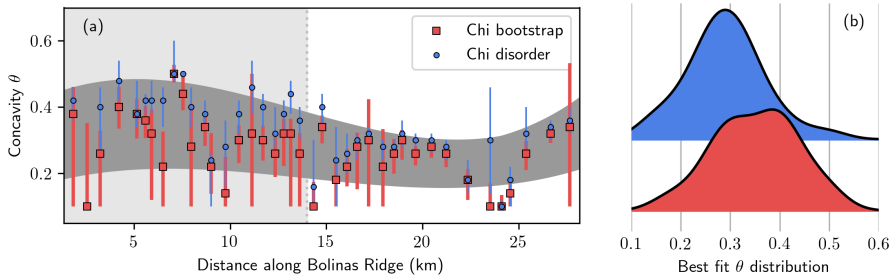
15

Figure 5: (a) Variation in θ derived using χ methods following [29, 28] along the Bolinas Ridge from NW to SE. Channel concavity generally decreases toward the zone inferred to have maximum uplift. Dark gray background shaded region indicative of a univariate spline fitted through the minima and maxima of each dataset for visualization purposes only. (b) Distribution of θ for both methods described by [29]. The median value determined using the bootstrap method ($\pm 1 median absolute deviation$) is $\theta = 0.31 \pm 0.1$, which was subsequently used to estimate k_{sn}. A Mann-Kendall test performed on both disorder and bootstrap concavity values indicates a statistically significant decrease in concavity with increasing distance (p values of 2×10^{-5} and 0.015, respectively).

individual catchments), we observed a distribution of k_{sn} similar to that derived by [6] (Figure 6). Channel steepness and catchment relief increase along the Bolinas Ridge from NW to SE. The scale of absolute values vary systematically due to use of different θ_{ref} ($\theta_{ref} = 0.45$ in [6]), and any slight differences likely

245 relate to the use of higher resolution topography in this study, and our objective approach to channel network extraction. Nevertheless, this spatial pattern of k_{sn} is expected to reflect channel erosion rates in response to differential uplift [6].

Erosion in the channel network sets the boundary conditions for hillslopes

250 [17], and we found that hillslope morphology also changes systematically along
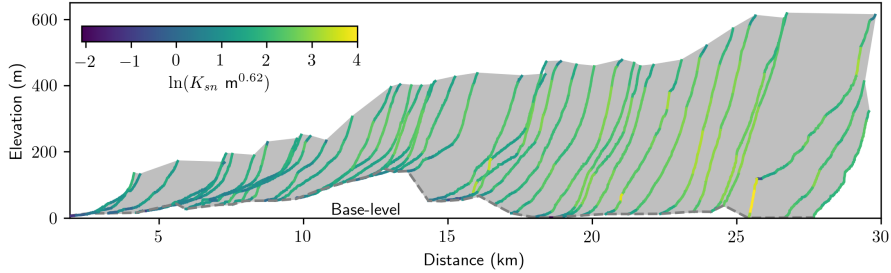
16

Figure 6: Longitudinal profiles of trunk channels from each catchment along the ridge, colored by channel steepness or k_{sn}. Yellow colors indicate relatively high values of k_{sn} and blue colors indicate low values. The channel steepness was normalized using a reference concavity of $\theta_{ref} = 0.31$. Gray shaded region indicates channel profile relief above base level.

the landform. In Figure 7 we plotted the distribution of k_{sn}, dimensionless hilltop erosion rate E^* and dimensionless hillslope relief R^* in each catchment with distance along the Bolinas Ridge. All three metrics tend to increase with distance from NW to SE.

₂₅₅ Figure 8 shows a positive correlation between the median channel steepness and both E^* and R^* for each basin, suggesting that channels, hillslope gradient, and hilltop curvatures are tightly coupled in their response to uplift along the ridge.

To explore hillslope morphology further, we plotted the 90th percentile con-₂₆₀ tour of E^* vs R^* point density for each catchment which allows us to visualize the shape of most of the data for a given basin while excluding outliers. Both dimensionless hilltop curvature E^* and dimensionless relief R^* increase with distance to the SE (Figure 9). The data broadly follow the steady-state prediction of Equation (10) (dashed line), however the E^* vs R^* data sit mostly
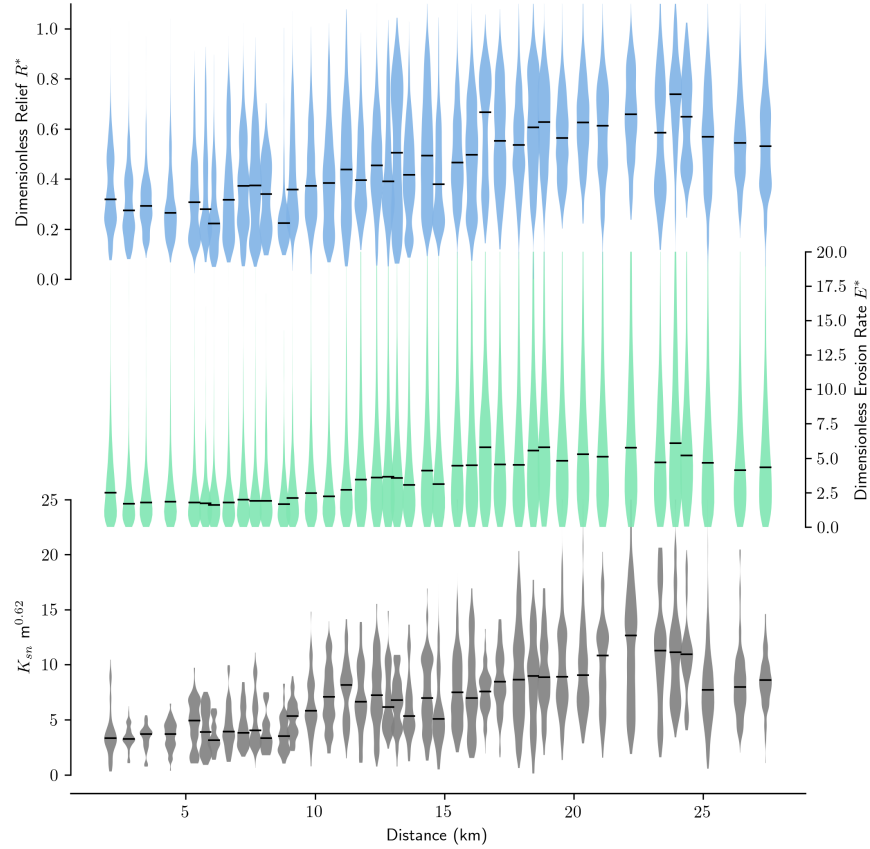
17

Figure 7: Relationship between median channel steepness (k_{sn}) and hillslope metrics for each of the basins along Bolinas Ridge. The relationship between k_{sn} and dimensionless hilltop erosion rate, E^*, is shown in blue, while the relationship between k_{sn} and dimensionless hillslope relief, R^*, is shown in green. The error bars span the 16th and 84th percentiles of the data in each catchment.

below the steady-state predictions in the NW, and mostly above in the SE.

Taking the orthogonal residuals in logarithmic E^* vs R^* space and plotting their distribution relative to the steady-state prediction of Equation (10) on a
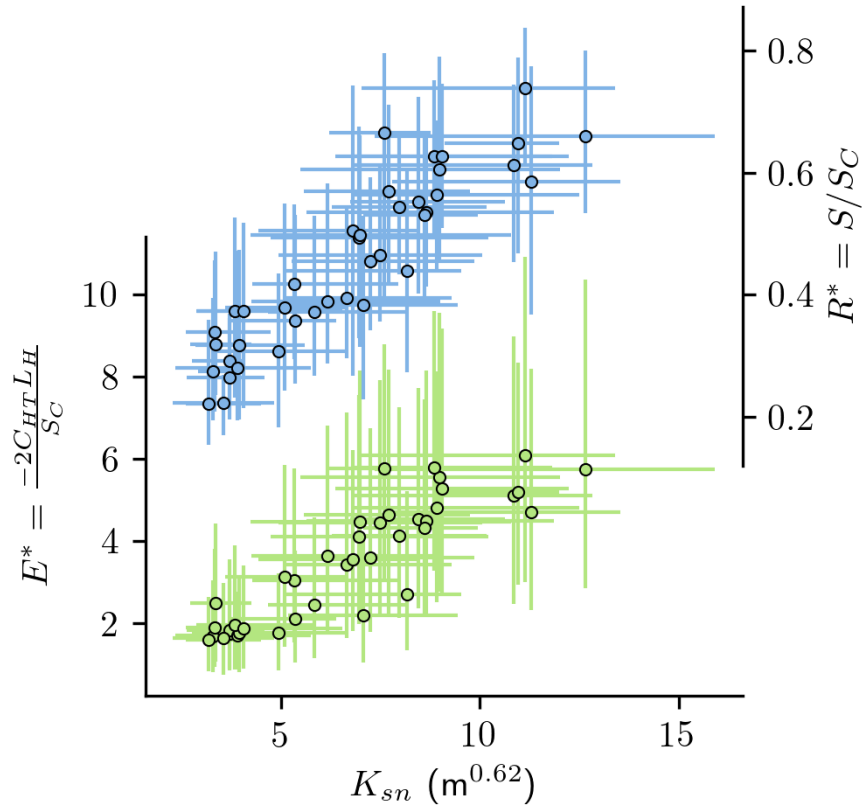
Figure 8: Relationship between median channel steepness (k_{sn}) and hillslope metrics for each of the basins along Bolinas Ridge. The relationship between k_{sn} and dimensionless hilltop erosion rate, E^*, is shown in blue, while the relationship between k_{sn} and dimensionless hillslope relief, R^*, is shown in green. The error bars span the 16th and 84th percentiles of the data in each catchment.

catchment-by-catchment basis (Figure 10) shows that the majority of residuals are negative at the NW end whereas the majority of residuals are positive to
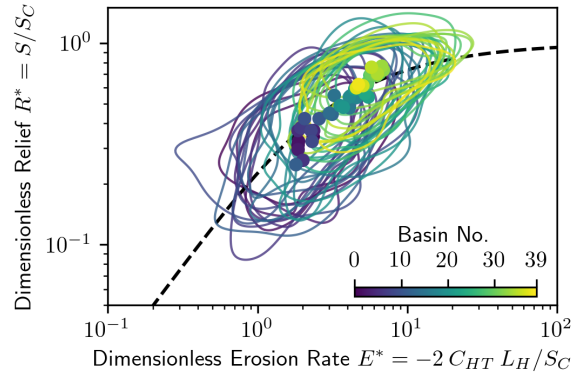270 the SE, where the magnitude of uplift is inferred to be higher.

Figure 9: Plot showing the progression of hillslope morphology along the length of the Bolinas Ridge. Colored lines are the 90th percentile contour of E^* vs R^* point density for traces within each catchment, where catchment numbers increase from NW to SE. Points are the median values in each catchment.
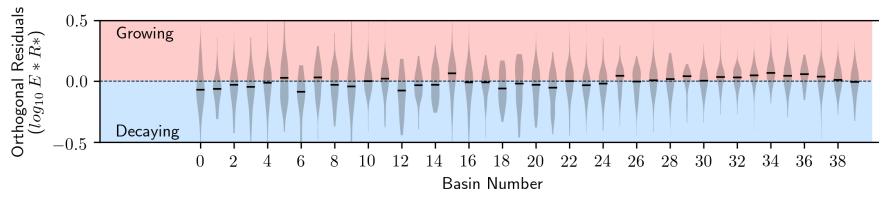

Figure 10: Distribution of hillslope morphology compared to steady-state predictions in basins along the length of the Bolinas Ridge. Where E^* or R^* values deviate from the steady-state predictions the landscape is inferred to be in a state of transience such that hillslopes are still adjusting to some recent increase or decrease in rates of channel lowering at their boundary.

6. Discussion

6.1. Variation in channel metrics

Our results (Figures 4–6) show that both planform channel geometry and longitudinal channel profiles respond to the inferred uplift rate gradient along Bolinas Ridge. Drainage density increases with distance to the SE along the ridge, corresponding with an overall decrease in hillslope lengths.

Analytical and numerical studies have shown that drainage density depends on the relative efficiency of channel erosion and hillslope sediment transport [e.g., 39, 40]. Drainage density increases with topographic relief (and by inference, erosion rates) when considering a threshold shear stress that must be exceeded for channel erosion to occur [e.g., 39], or when channel erosion is highly sensitive to channel slope [slope exponent greater than 1 in stream power incision model, see 40]. In fact these two scenarios are related, as *Gasparini and Brandon* [41] showed that a channel incision model that included a threshold term could be approximated with a slope exponent greater than unity. In either case, increased drainage density with channel gradients suggests that there are non-linear feedbacks between channel gradient and the channel incision rate, such that channel incision becomes highly efficient as channels steepen. This finding mirrors that of *Clubb et al.* [12], where sites with erosion rate data showed systematic increases in drainage density with erosion across a range of rock types and climates.

However, this positive correlation between drainage density and distance along the ridge is not evident toward the SE end of the ridge, where the basins

have the highest median channel steepness and hillslope relief (Figure 7). Previous work in high relief landscapes, such as the central Japanese mountains [42] and mountainous regions in California [43, 7], has found decreasing drainage density with increasing relief. These authors attributed this to the transition to debris flow hillslope processes in high relief landscapes, as slopes approach the angle of repose. Our approach to mapping the channel network does not distinguish between debris flow and fluvially-formed valleys and so the observed positive relationship between drainage density and relief along the Bolinas Ridge may alternatively be the result of increased efficiency of debris flows as a valley forming process. The lack of distinction between debris flow dominated and fluvially-formed valleys has implications for quantifying variation in channel concavity.

Examining the variation in the longitudinal channel profiles with uplift, we found that θ decreases with distance to the SW along Bolinas Ridge with the lowest values at around 22–26 km (Figure 5). This result is consistent between both the disorder [28] and bootstrap [29] methods of estimating concavity. Concavity had previously been suggested to be relatively insensitive to variation in uplift [1], however, a recently published analytical model for the evolution of transport-limited gravel-bed rivers predicts that channel concavity decreases with increasing uplift [44], which is consistent with our results. Alternatively, dependence of concavity on uplift may reflect the influence of non-fluvial valley forming processes on the upper part of the channel network in catchments that are uplifting most rapidly, as has also been suggested as the cause of spa-

22

tial variation in drainage density above. Debris flow processes operating in the upper reaches of valley networks can result in steep, planar valley long profiles, with a non-power law relationship between valley slope and drainage area [45]. Furthermore, recent studies have suggested that increased erosion rates are correlated with longer sections of the channel being dominated by debris flows [46, 47], which would reduce the overall apparent concavity of the channel network [28]. Numerous debris flows have been mapped in the area, with high concentrations of debris flows in the headwaters beginning at catchment 30 and above (approximately 18 km along the landform measured from Point Reyes Station) [48].

A reduction in concavity with uplift could also be the result of spatial gradients in uplift within individual catchments [49], but would require uplift rates to be highest near the catchment outlet in order to result in concavity values lower than typically expected ($\theta = 0.4 - 0.6$, [1]). Nevertheless, a relationship between channel concavity and uplift has not previously been demonstrated from field data, and future studies should seek to verify whether such a relationship exists in other landscapes.

In order to calculate channel steepness, we normalize each channel profile for $\theta = 0.31$, the median value estimated along the ridge. When this normalizing procedure is performed, we find a positive relationship between k_{sn} and distance along the ridge, similar to [6]. This approach of normalizing channel steepness to a reference concavity is performed routinely by many studies in tectonic geomorphology [e.g., 4, 5, 6, 1], and is important to ensure that k_{sn} values

23

are comparable between catchments. However, our results here highlight that channel concavity can be spatially heterogeneous with uplift rate, and this may impact the extraction of the absolute value of channel steepness metrics. This is a confounding challenge when concavity and channel steepness covary with uplift.

6.2. Variation in hillslope metrics

Catchment median hilltop curvature increases from NW to SE along the Bolinas Ridge (Figure 7). Assuming that diffusion-like processes dominate hillslope sediment transport, C_{HT} should be linearly proportional to erosion rates according to Equation 6. Assuming ρ_s/ρ_r=0.5, and an estimate for the sediment transport coefficient D=5 m^{2}ky $^{-1}$ [50], median C_{HT} values indicate erosion rates increasing from approximately 12 to 625 mm ky^{-1} from NW to SE along the Bolinas Ridge. Whilst there is evidence that hillslope transport may not be purely diffusion-like in this landscape but instead have some dependence on soil thickness [50], analytical solutions for hillslope morphology governed by depth-dependent soil creep suggest that C_{HT} is still a sensitive indicator of erosion rates in such cases [51]. Furthermore, calculation of $\nabla^2 z$ is sensitive to the grid resolution of the topographic data [38], such that for narrow hilltops and relatively coarse resolution topography (3 m) we may be underestimating values of C_{HT}. Thus, these erosion rate estimates may be considered conservative. These erosion rate estimates could in future be compared to catchment-averaged erosion rates quantified using cosmogenic isotopes.

Under the assumption that hillslopes are in steady-state (lowering in concert

24

with their bounding channels), dimensionless hillslope morphology can be predicted by the nonlinear sediment transport law (Equation 5) as shown by the dashed line in Figure 9 (Equation 10). Where real hillslope morphology plots above this steady-state prediction, this is indicative of landscapes that are growing in relief, yet hillslopes that plot below the steady-state prediction indicate that relief is declining [17, 11]. The progression of orthogonal residuals in E^* vs R^* space for each catchment (Figure 10) from predominantly negative in the NW to predominantly positive in the SE suggests that catchments previously inferred to be experiencing low uplift rates in the NW are declining in relief, while catchments in the SE are experiencing rejuvenation and growing relief.

6.3. Coupling channels and hillslopes

Our results show a clear coupling of k_{sn}, E^* and R^* along the Bolinas Ridge (Figure 8). This suggests that channel and hillslope metrics are tightly linked at the catchment scale, despite the expectation that the response of hillslopes should lag behind that of channels [17]. The broad coupling suggests that the uplift gradient must have persisted for long enough that both channels and hillslopes have had time to adapt, although numerical modeling suggests that increases in channel erosion rates may only be detectable on hillslopes for at most tens of thousands of years [32].

7. Conclusions

We analyzed coupled hillslope-channel morphology from high-resolution topography along an uplift gradient proximal to the San Andreas Fault in Cal-

25

₃₈₅ ifornia. Multiple landscape metrics are shown to increase with inferred relative uplift rates, including drainage density (hillslope lengths shorter with more rapid uplift/incision), the concavity of channel profiles, hillslope relief and hilltop curvature. These metrics are all correlated with channel steepness, which has previously been used as a proxy for uplift rates [6]. We suggest that increasing drainage density and decreased channel concavity with uplift rate are the result of non-fluvial valley forming processes operating in the headwaters of the valley network. Catchments inferred to be experiencing highest uplift rates have hillslope morphology that suggests landscape relief is still growing, but in the NW catchments with lower relief have hillslope morphology consistent with landscape relaxation. Our results integrate several previously published analytical approaches to topographic analysis, that combined, allow us to identify trends in landscape form in inherently noisy topographic data that was previously not possible.

8. Code and Data Availability

₄₀₀ Software used for the analysis in this contribution is located at `https://doi.org/10.5281/zenodo.3245040` [52]. Documentation with instructions on how to install and run the software can be found at `https://doi.org/10.5281/zenodo.2560223` [53]. The parameter files, software output, and plotting scripts producing the figures for this paper are available at `https://https://doi.org/10.5525/gla.researchdata.835` [54]. All topographic data used in this contribution is available through `https://viewer.nationalmap.gov/basic/`

26

(last accessed 11th June 2019).

9. Author Contributions

SMM, FJC and SWDG led various aspects of software development, with ₄₁₀ contributions from all authors. MDH ran the software and analysed results, with guidance and contributions from all authors. MDH led writing the manuscript following discussions with, and inputs from all other authors.

10. Acknowledgments

₄₁₅ [1] E. Kirby, K. X. Whipple, Expression of active tectonics in erosional land-scapes, Journal of Structural Geology 44 (2012) 54 – 75. `doi:https://doi.org/10.1016/j.jsg.2012.07.009`.

[2] K. X. Whipple, G. E. Tucker, Dynamics of the stream-power river inci-sion model: Implications for height limits of mountain ranges, landscape ₄₂₀ response timescales, and research needs, Journal of Geophysical Research 104 (B8) (1999) 17661. `doi:10.1029/1999JB900120`.

[3] A. C. Whittaker, How do landscapes record tectonics and climate?, Litho-sphere 4 (2) (2012) 160–164. `doi:10.1130/RF.L003.1`.

[4] N. P. Snyder, K. X. Whipple, G. E. Tucker, D. J. Merritts, Stream profiles ₄₂₅ in the Mendocino triple junction region, northern California, GSA Bul-

letin 112 (8) (2000) 1250–1263. `doi:10.1130/0016-7606(2000)112<1250:` `lrttfd>2.3.co;2`.

[5] C. Wobus, K. X. Whipple, E. Kirby, N. Snyder, N. Johnson, K. Spyropolou, B. Crosby, D. Sheehan, Tectonics from topography: procedures, promise, and pit- falls, in: Tectonics, Climate, and Landscape Evolution, Vol. 398, Geological Society of America, 2006, pp. 55–74.

[6] E. Kirby, C. Johnson, K. Furlong, A. Heimsath, Transient channel incision along Bolinas Ridge, California: Evidence for differential rock uplift adjacent to the San Andreas fault, Journal of Geophysical Research: Earth Surface 112 (3). `doi:10.1029/2006JF000559`.

[7] R. A. DiBiase, K. X. Whipple, A. M. Heimsath, W. B. Ouimet, Landscape form and millennial erosion rates in the San Gabriel Mountains, CA, Earth and Planetary Science Letters 289 (1-2) (2010) 134–144. `doi:10.1016/j.` `epsl.2009.10.036`.

[8] V. Vanacker, F. von Blanckenburg, G. Govers, A. Molina, B. Campforts, P. W. Kubik, Transient river response, captured by channel steepness and its concavity, Geomorphology 228 (2015) 234–243. `doi:10.1016/j.` `geomorph.2014.09.013`.

[9] M. D. Hurst, S. M. Mudd, R. Walcott, M. Attal, K. Yoo, Using hilltop curvature to derive the spatial distribution of erosion rates, Journal of Geophysical Research: Earth Surface 117 (2). `doi:10.1029/2011JF002057`.

[10] R. A. DiBiase, A. M. Heimsath, K. X. Whipple, Hillslope response to tectonic forcing in threshold landscapes, Earth Surface Processes and Landforms 37 (8) (2012) 855–865. `doi:10.1002/esp.3205`.

[11] S. W. D. Grieve, S. M. Mudd, M. D. Hurst, D. T. Milodowski, A nondimensional framework for exploring the relief structure of landscapes, Earth Surface Dynamics 4 (2016) 309–325. `doi:10.5194/esurf-4-309-2016`.

[12] F. J. Clubb, S. M. Mudd, M. Attal, D. T. Milodowski, S. W. Grieve, The relationship between drainage density, erosion rate, and hilltop curvature: Implications for sediment transport processes, Journal of Geophysical Research: Earth Surface 121 (10) (2016) 1724–1745, 2015JF003747. `doi:10.1002/2015JF003747`.

[13] S. F. Gallen, K. W. Wegmann, K. L. Frankel, S. Hughes, R. Q. Lewis, N. Lyons, P. Paris, K. Ross, J. B. Bauer, A. C. Witt, Hillslope response to knickpoint migration in the southern appalachians: implications for the evolution of post-orogenic landscapes, Earth Surface Processes and Landforms 36 (9) (2011) 1254–1267. `doi:10.1002/esp.2150`.

[14] J. J. Roering, J. W. Kirchner, W. E. Dietrich, Hillslope evolution by nonlinear, slope-dependent transport: Steady state morphology and equilbrium adjustment timescales, Journal of Geophysical Research-Solid Earth 107 (B3) (2002) 16499. `doi:10.1029/2002jb001822`.

[15] G. L. Bennett, S. R. Miller, J. J. Roering, D. A. Schmidt, Landslides, threshold slopes, and the survival of relict terrain in the wake of the Men-

docino Triple Junction, Geology 44 (5) (2016) 363–366. `doi:10.1130/`
`G37530.1.`

[16] C. M. Shobe, G. E. Tucker, R. S. Anderson, Hillslope-derived blocks retard river incision, Geophysical Research Letters 43 (10) (2016) 5070–5078. `doi:` `10.1002/2016GL069262.`

[17] M. D. Hurst, S. M. Mudd, M. Attal, G. Hilley, Hillslopes Record the Growth and Decay of Landscapes, Science 341 (6148) (2013) 868–871. `doi:10.` `1126/science.1241791.`

[18] L. Goren, M. Fox, S. D. Willett, Tectonics from fluvial topography using formal linear inversion: Theory and applications to the Inyo Mountains, California, Journal of Geophysical Research: Earth Surface 119 (8) (2014) 1651–1681. `doi:10.1002/2014JF003079.`

[19] J. J. Roering, J. T. Perron, J. W. Kirchner, Functional relationships between denudation and hillslope form and relief, Earth and Planetary Science Letters 264 (1-2) (2007) 245–258. `doi:10.1016/j.epsl.2007.09.035.`

[20] S. M. Mudd, M. Attal, D. T. Milodowski, S. W. D. Grieve, D. A. Valters, A statistical framework to quantify spatial variation in channel gradients using the integral method of channel profile analysis, Journal of Geophysical Research: Earth Surface 119 (2) (2014) 138–152. `doi:` `10.1002/2013JF002981.`

[21] S. W. D. Grieve, S. M. Mudd, M. D. Hurst, How long is a hillslope? (2016). `doi:10.1002/esp.3884.`

[22] G. Gilbert, Geology of the henry mountains, USGS Unnumbered Series, Government Printing Office, Washington, D.C. (1877).

[23] M. E. Morisawa, Quantitative Geomorphology of Some Watersheds in the Appalachian Plateau, Geological Society of America Bulletin 73 (9) (1962) 1025–1046. doi:10.1130/0016-7606(1962)73[1025:QGOSWI]2.0.CO;2.

[24] W. B. Ouimet, K. X. Whipple, D. E. Granger, Beyond threshold hillslopes: Channel adjustment to base-level fall in tectonically active mountain ranges, Geology 37 (7) (2009) 579–582. doi:10.1130/G30013A.1.

[25] M. A. Harel, S. M. Mudd, M. Attal, Global analysis of the stream power law parameters based on worldwide 10be denudation rates, Geomorphology 268 (2016) 184–196. doi:10.1016/j.geomorph.2016.05.035.

[26] L. Royden, J. Perron, Solutions of the stream power equation and application to the evolution of river longitudinal profiles, Journal of Geophysical Research: Earth Surface 118 (2) (2013) 497–518. doi:10.1002/jgrf.20031.

[27] K. X. Whipple, R. A. DiBiase, W. B. Ouimet, A. M. Forte, Preservation or piracy: Diagnosing low-relief, high-elevation surface formation mechanisms, Geology 45 (1) (2017) 91–94. doi:10.1130/G38490.1.

[28] S. Hergarten, J. Robl, K. Stwe, Tectonic geomorphology at small catchment sizes extensions of the stream-power approach and the χ method, Earth Surface Dynamics 4 (1) (2016) 1–9. doi:10.5194/esurf-4-1-2016.

[29] S. M. Mudd, F. J. Clubb, B. Gailleton, M. D. Hurst, How concave are river channels?, Earth Surface Dynamics 6 (2) (2018) 505–523. `doi:10.5194/esurf-6-505-2018`.

[30] J. J. Roering, J. W. Kirchner, W. E. Dietrich, Evidence for nonlinear, diffusive sediment transport on hillslopes and implications for landscape morphology, Water Resources Research 35 (3) (1999) 853–870. `doi:10.1029/1998WR900090`.

[31] M. D. Hurst, S. M. Mudd, K. Yoo, M. Attal, R. Walcott, Influence of lithology on hillslope morphology and response to tectonic forcing in the northern Sierra Nevada of California, Journal of Geophysical Research: Earth Surface 118 (2) (2013) 832–851. `doi:10.1002/jgrf.20049`.

[32] S. M. Mudd, Detection of transience in eroding landscapes, Earth Surface Processes and Landforms 42 (1) (2017) 24–41. `doi:10.1002/esp.3923`.

[33] J. C. Clark, E. E. Brabb, Geology of point reyes national seashore and vicinity, california: a digital database, USGS Numbered Series 97-456, U.S. Geological Survey, (1997).

[34] K. Grove, L. S. Sklar, A. M. Scherer, G. Lee, J. Davis, Accelerating and spatially-varying crustal uplift and its geomorphic expression, San Andreas Fault zone north of San Francisco, California, Tectonophysics 495 (3) (2010) 256–268. `doi:10.1016/j.tecto.2010.09.034`.

[35] C. Daly, G. Taylor, W. Gibson, The Prism Approach to Mapping Precipi-

tation and Temperature, 10th AMS Conference on Applied Climatology 1 (1997) 1–4.

[36] J. D. Pelletier, A robust, two-parameter method for the extraction of drainage networks from high-resolution digital elevation models (DEMs): Evaluation using synthetic and real-world DEMs, Water Resources Research 49 (1) (2013) 75–89. `doi:10.1029/2012WR012452`.

[37] F. J. Clubb, S. M. Mudd, D. T. Milodowski, M. D. Hurst, L. J. Slater, Objective extraction of channel heads from high-resolution topographic data, Water Resources Research 50 (5) (2014) 4283–4304. `doi:10.1002/2013WR015167`.

[38] S. W. D. Grieve, S. M. Mudd, D. T. Milodowski, F. J. Clubb, D. J. Furbish, How does grid-resolution modulate the topographic expression of geomorphic processes?, Earth Surface Dynamics 4 (3) (2016) 627–653. `doi:10.5194/esurf-4-627-2016`.

[39] A. D. Howard, Badland Morphology and Evolution: Interpretation Using a Simulation Model, Earth Surface Processes and Landforms 22 (3) (1997) 211–227. `doi:10.1002/(SICI)1096-9837(199703)22:3<211::AID-ESP749>3.0.CO;2-E`.

[40] G. E. Tucker, R. L. Bras, Hillslope Processes , Drainage Density , and Landscape Morphology Hillslope Processes , Drainage Density , and Landscape Morphology, Water Resources Research 34 (617) (1998) 0–52.

[41] N. M. Gasparini, M. T. Brandon, A generalized power law approximation for fluvial incision of bedrock channels, Journal of Geophysical Research: Earth Surface 116 (F2). `doi:10.1029/2009JF001655`.

[42] T. Oguchi, Drainage Density and Relative Relief in Humid Steep Mountains with Frequent Slope Failure, Earth Surface Processes and Landforms 22 (2) (1997) 107–120. `doi:10.1002/(SICI)1096-9837(199702)22:2<107::AID-ESP680>3.0.CO;2-U`.

[43] P. J. Talling, M. J. Sowter, Drainage density on progressively tilted surfaces with different gradients, Wheeler Ridge, California, Earth Surface Processes and Landforms 24 (9) (1999) 809–824. `doi:10.1002/(SICI)1096-9837(199908)24:9<809::AID-ESP13>3.0.CO;2-R`.

[44] A. D. Wickert, T. F. Schildgen, Long-profile evolution of transport-limited gravel-bed rivers, Earth Surface Dynamics 7 (1) (2019) 17–43. `doi:https://doi.org/10.5194/esurf-7-17-2019`.

[45] J. D. Stock, W. E. Dietrich, Valley Incision by Debris Flows: Evidence of a Topographic Signature, Water Resour. Res. 39 (4) (2003) 1089–1113. `doi:10.1029/2001WR001057`.

[46] B. D. Penserini, J. J. Roering, A. Streig, A morphologic proxy for debris flow erosion with application to the earthquake deformation cycle, cascadia subduction zone, usa, Geomorphology 282 (2017) 150 – 161. `doi:https://doi.org/10.1016/j.geomorph.2017.01.018`.

[47] R. A. DiBiase, M. W. Rossi, A. B. Neely, Fracture density and grain size controls on the relief structure of bedrock landscapes proposal, Geology 46 (5) (2018) 1–14. `doi:10.1130/G40006.1`.

[48] S. D. Ellen, R. K. Mark, G. F. Wieczorek, D. W. Wentworth, D. W. Ramsay, T. E. May, San Fransisco Bay region landslide folio part E– map of debris–flow source areas in the San Francisco Bay region, California, United States Geological Survey, Washington D.C., 1997.

[49] E. Kirby, K. Whipple, Quantifying differential rock-uplift rates via stream profile analysis, Geology 29 (5) (2001) 415. `doi:10.1130/0091-7613(2001)029<0415:QDRURV>2.0.CO;2`.

[50] A. M. Heimsath, D. J. Furbish, W. E. Dietrich, The illusion of diffusion: Field evidence for depth-dependent sediment transport, Geology 33 (12) (2005) 949–952. `doi:10.1130/G21868.1`.

[51] J. J. Roering, How well can hillslope evolution models "explain" topography? Simulating soil transport and production with high-resolution topographic data, Bulletin of the Geological Society of America 120 (9-10) (2008) 1248–1262. `doi:10.1130/B26283.1`.

[52] S. M. Mudd, F. J. Clubb, S. W. D. Grieve, D. T. Milodowski, M. D. Hurst, B. Gailleton, D. A. Valters, Lsdtopotools2 (Jun. 2019). `doi:10.5281/zenodo.3245041`.

[53] S. M. Mudd, F. J. Clubb, B. Gailleton, S. W. D. Grieve, D. A. Valters, M. D.

Hurst, Lsdtopotools documentation (Feb. 2019). `doi:10.5281/zenodo.2560224`.

[54] M. D. Hurst, S. W. D. Grieve, F. J. Clubb, S. M. Mudd, Detection of channel-hillslope coupling along a tectonic gradient, Data Collection`doi:10.5525/gla.researchdata.835`.